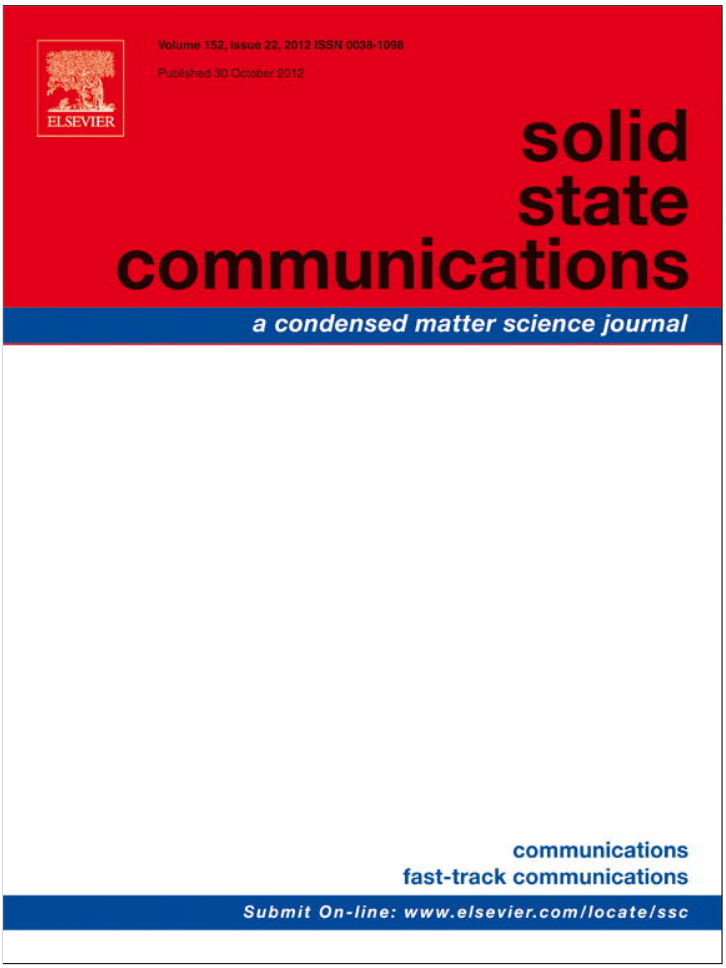

Solid State Communications 152 (2012) 2036–2039

Contents lists available at SciVerse ScienceDirect

Solid State Communications

journal homepage: www.elsevier.com/locate/ssc

Bipolar resistive switching in $BiFe_{0.95}Mn_{0.05}O_3$ films

Qingyu Xu [a,b,*], Xueyong Yuan [a], Yanqiang Cao [c], Lifang Si [a], Di Wu [c]

[a] Department of Physics, Southeast University, Nanjing, Jiangsu 211189, China
[b] Key Laboratory of MEMS of the Ministry of Education, Southeast University, Nanjing 210096, China
[c] Department of Materials Science and Engineering, Nanjing University, Nanjing 210008, China

ARTICLE INFO

Article history:
Received 29 June 2012
Received in revised form
23 August 2012
Accepted 24 August 2012
by Xianhui Chen
Available online 2 September 2012

Keywords:
A. Magnetic films and multilayers
A. Ferroelectrics
B. Laser processing
D. Electronic transport

ABSTRACT

$BiFe_{0.95}Mn_{0.05}O_3$ films were prepared on $LaNiO_3$ buffered surface oxidized Si substrates by pulsed laser deposition. With silver glue dots prepared on the $BiFe_{0.95}Mn_{0.05}O_3$ films, forming-free bipolar resistive switching (BRS) behavior has been observed in $LaNiO_3/BiFe_{0.95}Mn_{0.05}O_3$/Ag devices with the resistance ratio of the high resistance state (HRS) to the low resistance state (LRS) of about 3. With voltage of above 6.5 V applied on the top Ag electrode, a forming process with drastic increase of R_{HRS} has been observed. The BRS behavior persists, and the R_{HRS}/R_{LRS} ratio is strongly enhanced to about 10^2. The conduction mechanisms of the LRS and HRS have been verified to be Ohmic and trap controlled space charge limited current (SCLC), respectively. The model based on the formation/rupture of the conducting filaments formed by O vacancies has been applied to explain the BRS behavior.

1. Introduction

Resistive random access memory (RRAM) based on the resistive switching (RS) effect has been considered to be one of the potential candidates for the next generation nonvolatile memory devices and attracted intensive research interests due to its high operation speed, high storage density, and low energy consumption [1]. The RS behavior is that the resistance R can be reversibly switched between the high resistance state (HRS) and the low resistance state (LRS) by the stimulation of the external electric field, and can be categorized to unipolar resistive switching (URS) and bipolar resistive switching (BRS), according to the applied bias polarity [2]. The RS behavior has been intensively studied in oxides, such as ZnO, TiO_2, $SrTiO_3$, etc. [2–4]. $BiFeO_3$ is a widely studied multiferroic material, due to its above room temperature ferroelectric Curie temperature ($T_C \sim 1143$ K) and antiferromagnetic Néel temperature ($T_N \sim 643$ K) [5]. Besides the intensively studied multiferroic properties, RS behavior was first observed in epitaxial Ca-doped $BiFeO_3$ single crystalline film [6]. And later both URS and BRS behavior have been observed in polycrystalline $BiFeO_3$ films, and various mechanisms such as formation/rupture of the conducting filaments, Schottky emission with modification of the depletion width, etc., have been suggested [7,8].

In this paper, we report the RS behavior in $LaNiO_3$ (LNO)/$BiFe_{0.95}Mn_{0.05}O_3$ (BFMO)/Ag devices. A forming-free BRS with R_{HRS}/R_{LRS} ratio of about 3 has been observed. Furthermore, with applied voltage above 6.5 V on the top Ag electrode, the R_{HRS} increases abruptly one order larger and the R_{LRS} decreases slightly, the R_{HRS}/R_{LRS} ratio has been significantly enhanced to about 10^2.

2. Experimental details

BFMO films have been deposited on surface oxidized Si substrates at substrate temperature T_s of 700 °C by pulsed laser deposition (PLD) using a KrF excimer laser with frequency of 5 Hz from an analytically pure $Bi_{1.04}Fe_{0.95}Mn_{0.05}O_3$ target. Before the deposition of BFMO film, LNO buffer layer was first deposited at T_s of 850 °C in an O_2 ambient with pressure of 40 Pa. The O_2 pressure during the deposition of BFMO films was kept to be 2 Pa. Then the O_2 pressure was increased to 1×10^5 Pa. The T_s decreased to 550 °C and the samples were annealed for 30 min. The film thickness was controlled by the number of laser pulse (1000 in this paper) with pulse energy of 300 mJ. The structure of the film was studied by X-ray diffraction (XRD, Rigaku), scanning electron microscope (SEM, FEI) and X-ray photoelectron spectroscopy (XPS, ThermoFisher SCIENTIFIC) with Al Kα X-ray source ($h\nu$ = 1486.6 eV). The current-voltage (I–V) measurements were carried out using a Keithley 2400 SourceMeter and 2182A Nanovoltmeter at room temperature. Silver glue dots with a diameter of ca. 1 mm were used as top electrodes. During the voltage sweep mode, the

* Corresponding author at: Department of Physics, Southeast University Nanjing, Jiangsu 211189, China. Tel.: +86 25 52090600x8308; fax: +86 25 52090600x8203.
E-mail address: xuqingyu@seu.edu.cn (Q. Xu).

0038-1098/$ - see front matter © 2012 Elsevier Ltd. All rights reserved.
http://dx.doi.org/10.1016/j.ssc.2012.08.023

bias was defined as positive when the current flowed from the bottom $LaNiO_3$ electrode through the film to the top Ag electrode.

3. Results and discussion

Fig. 1 shows the XRD pattern of the BFMO film. It can be seen that except for the diffraction peaks from LNO buffer layer (marked by "∗" in red), all peaks can be indexed as $BiFeO_3$ in R3c structure, and only a small peak (marked by a blue arrow) corresponding to $Bi_2Fe_4O_9$ impurity phase was observed. This suggests that LNO is an effective buffer layer for the crystallization of BFMO, as our previous report [9]. The microstructure of the film was studied by SEM, and the cross-sectional image is shown in the inset of Fig. 1(a). The thicknesses of the BFMO and LNO are very uniform and can be determined to be about 80 and 130 nm, respectively. Generally Mn ions have been doped in $BiFeO_3$ to reduce the leakage current [10]. The XPS spectrum of doped Mn ions was taken to explore the electronic structure, as shown in Fig. 1(b). The XPS spectra were referenced to the surface impurity C 1s line (284.8 eV) binding energy [11]. The curve is slightly noisy due to the low concentration of Mn ions, and multi peaks are difficult to fit the curve. As can be seen, the peak position of Mn $2P_{3/2}$ is 641.7 eV. As the binding energy of Mn^{2+} in MnO is about 641 eV, and that of Mn^{4+} in MnO_2 is about 642 eV, it is suggested that at least partial doped Mn ions are in +4 valence state [12].

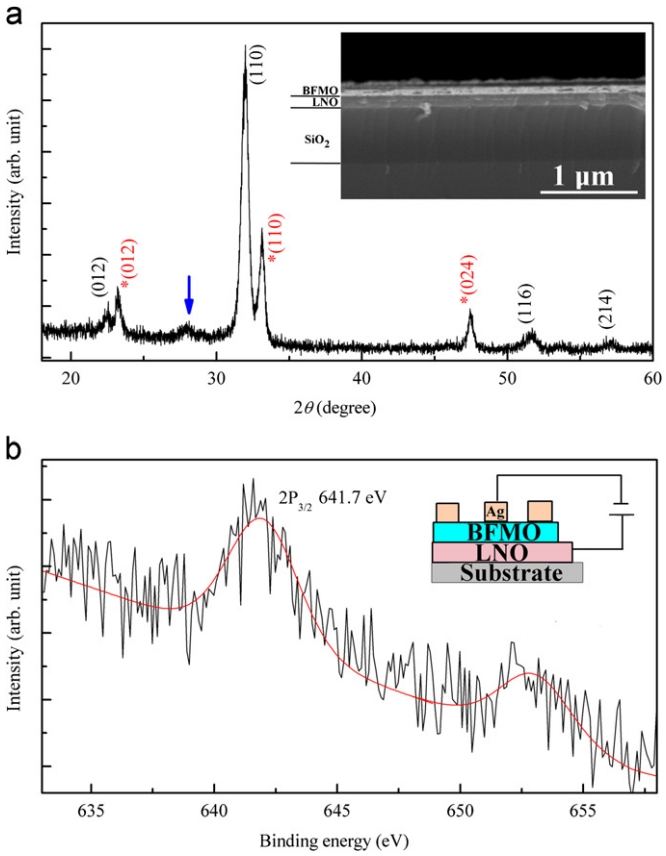

Fig. 1. (Color online) (a) XRD pattern of BFMO film on LNO buffer layer. The diffraction peaks of LNO are marked by "∗" in red, the blue arrow indicates the $Bi_2Fe_4O_9$ impurity phase, and the inset shows the cross-sectional SEM image. (b) the Mn 2P XPS spectrum, the inset shows the schematic drawing of the *I–V* measurement system.

The schematic LNO/BFMO/Ag device structure is illustrated in the inset of Fig. 1(b), and the *I–V* cycles are plotted in Fig. 2. The device is initially in the HRS. By sweeping the bias voltage to about 1 V, the device switches to the LRS via the set process. As the device turns to the LRS, the current suddenly increases. To protect the devices, a compliance current of 1 mA was selected for the set processes. A subsequent sweep with negative voltage switches the device back to the HRS, which is called the reset process. As can be seen, the device exhibits the typical characteristics of BRS. Generally, a forming process is needed, which needs higher voltage to switch the devices from HRS to LRS than that in the subsequent set processes [13,14]. As can be seen in Fig. 2, the forming voltage is almost the same as the set voltage, indicating that the device is forming-free [15]. However, the R_{HRS}/R_{LRS} ratio is only about 3. The inset shows the typical *I–V* curves of the set and reset processes plotted in the log–log scale. The *I–V* curves of LRS exhibit a linear Ohmic behavior with a slope close to 1. This is consistent with the conducting filament model [16,17]. Fitting results of the HRS shows a linear dependence on voltage with a slope of around 1 at low voltage (Ohmic), and close to 2 at high voltage, the typical trap controlled space charge limited conduction (SCLC) [18]. We also tried to fit the *I–V* curves of LRS and HRS with other mechanisms, such as Schottky emission, Poole–Frenkel emission and Fowler–Nordeim tunneling [18], but all failed.

With the sweep of negative bias, only a small loop can be observed, and the device gradually changes from LRS to HRS. Interestingly, with further increasing the sweep bias up to above −6.5 V without the compliance current, a sudden drop of the current can be observed, indicating the drastically increase of the resistance, as shown in Fig. 3. We call this a negative forming process, for a new BRS can be observed with the reset voltage (∼ −2 V) much smaller than the forming voltage. The set voltage is the same as the set voltage of previous BRS. The R_{HRS}/R_{LRS} ratio significantly increases to about 10^2, which is almost 2 orders larger. Fig. 4 shows the *I–V* curves of LRS and HRS plotted in log–log scale. The LRS shows the Ohmic conducting with slope close to 1. The HRS shows the Ohmic conducting at low voltage with slope close to 1, and SCLC mechanism with slope close to 2. This suggests the conducting filament model. We further test the retention property of the device at room temperature. Both the HRS and LRS are very stable for more than 3000 s without degradation (Fig. 5).

We replot the *I–V* curves of the LRS and HRS before and after the negative forming process together in log–log scale in Fig. 6. It can be clearly seen that the after the negative forming process,

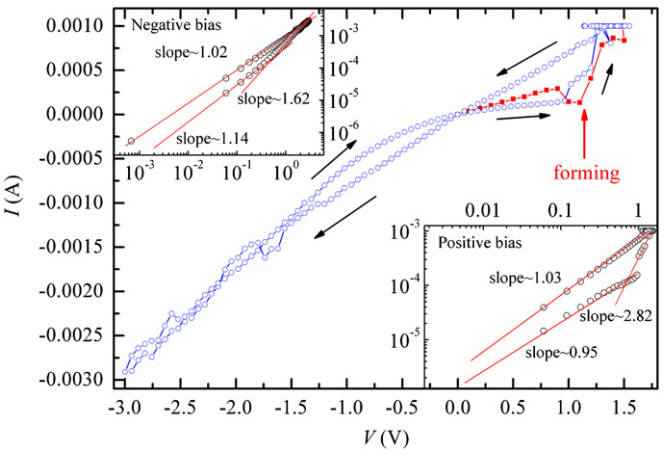

Fig. 2. (Color online) The typical BRS characteristics, the inset shows the set and reset *I–V* curves in log–log scale.

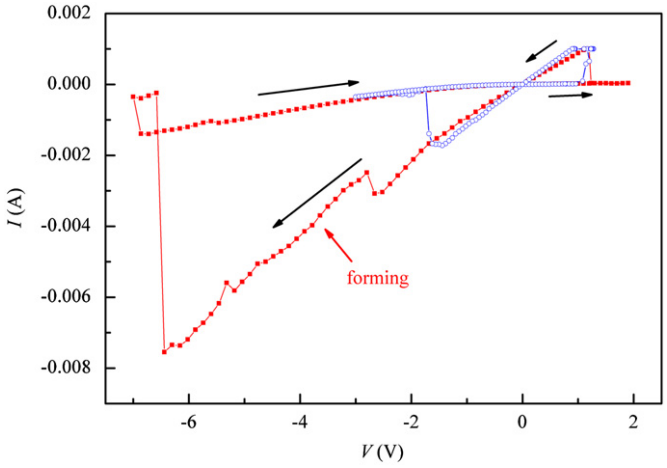

Fig. 3. (Color online) The typical BRS characteristics after the negative forming process.

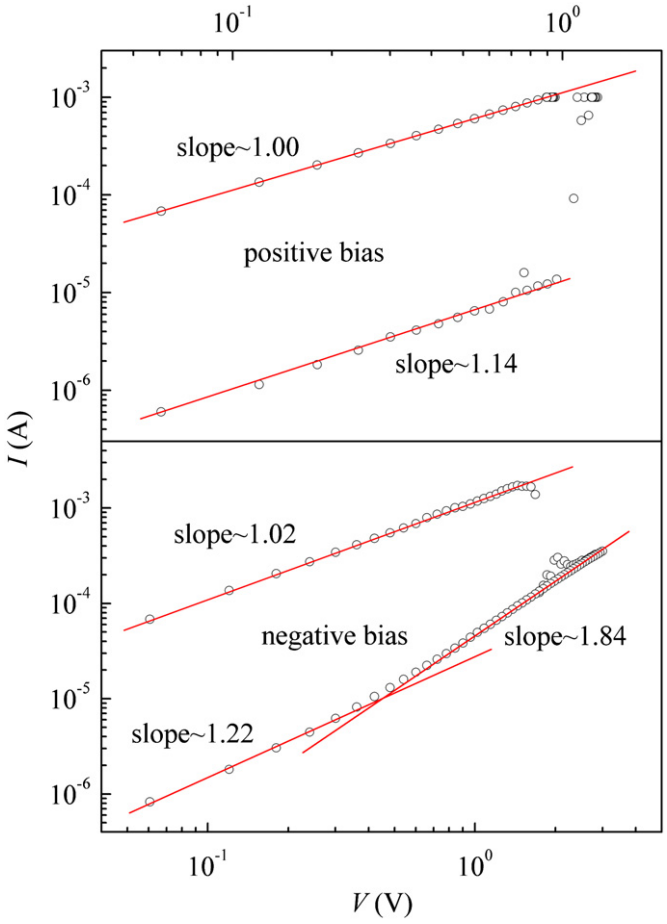

Fig. 4. (Color online) The set and reset *I*–*V* curves in log–log scale after the negative forming process.

the R_{HRS} increases drastically of more than 1 order, while the R_{LRS} decreases slightly. A schematic diagram (Fig. 7) is used to explain the sequence. Due to the large amount of grain boundaries, the fresh BFMO film is most likely to be in an HRS sate (Fig. 7(a)) [8]. The O vacancies have been generally considered to be the origin of the leakage current in $BiFeO_3$ [19]. However, as reported by Yang et al. that the diffusivity of O vacancies is very slow [6], the formation of the conducting filaments by the shift of O vacancies

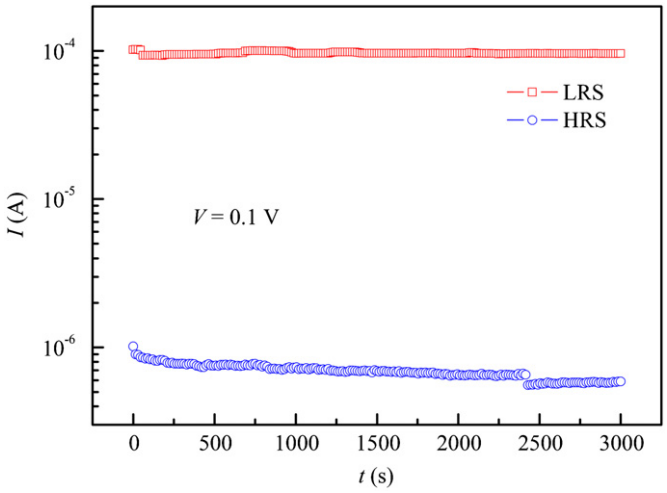

Fig. 5. (Color online) Retention of the HRS and LRS at room temperature with reading voltage of 0.1 V after the negative forming process.

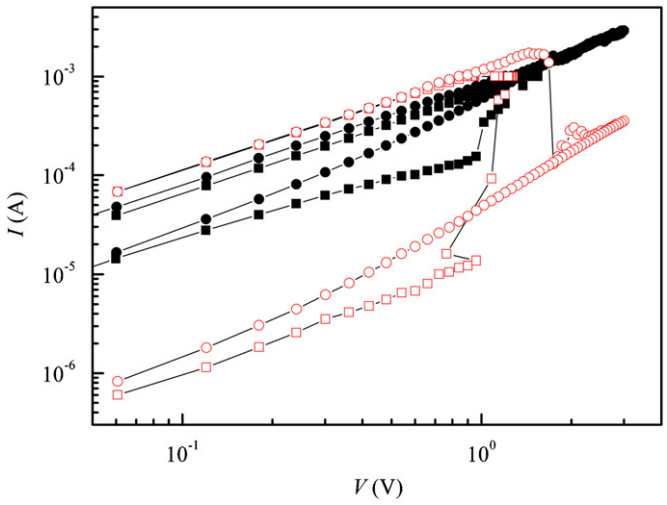

Fig. 6. (Color online) The set (square) and reset (circle) *I*–*V* curves in log–log scale before (filled symbols) and after (open symbols) the negative forming process.

from anode to cathode seems to be impossible. The distribution of the O vacancies in grain boundaries is different from that in grain interiors. With a high positive field applied, O vacancies will redistribute and conducting path might be formed across grain boundaries, due to the shift of the O vacancies to the grain boundaries from the neighboring sites (Fig. 7(b)). With negative voltage applied, the O vacancies will shift away, and the conducting channels are destroyed (Fig. 7(c)). Due to slight redistribution of O vacancies around the grain boundaries, the R_{HRS}/R_{LRS} ratio is small. Because of the random distribution of grain boundaries, there are narrowest regions in the conducting filaments, as indicated by the arrow in Fig. 7. This is the bottleneck for the conduction in the conducting filaments, where the highest electrical field will be applied and highest Joule heating will be generated. With the combination of the electrical field and Joule heating, the O vacancies might overcome the barriers, and shift farther away from the local sites with large enough voltage applied (Fig. 7(d)). Thus, much higher R_{HRS} can be achieved. With the redistribution of the O vacancies under high electrical field, more O vacancies might shift to the grain boundaries, especially at the bottleneck (Fig. 7(e)). Thus, the R_{LRS} becomes smaller and

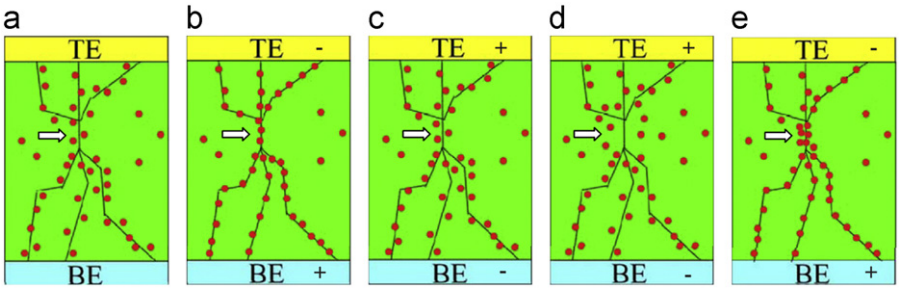

Fig. 7. (Color online) Schematic diagrams of resistive switching mechanism: (a) the fresh sample; (b) the set process and (c) the reset process before the negative forming process, (d) the negative forming process, (e) the set process after the negative forming process. The arrow indicates the bottleneck in the conducting filaments, the red circles indicate the O vacancies, and the lines indicate the grain boundaries.

much higher R_{HRS}/R_{LRS} ratio has been achieved after the negative forming.

4. Conclusions

In summary, LNO/BFO/Ag devices have been prepared, and forming-free BRS behavior has been observed with small R_{HRS}/R_{LRS} ratio of about 3. With voltage of above 6.5 V applied on the top Ag electrode, a forming process with drastic increase of R_{HRS} has been observed. The devices possess BRS behavior, and the R_{HRS}/R_{LRS} ratio is strongly enhanced to about 10^2. The conduction mechanisms of LRS and HRS were verified to be Ohmic and SCLC, respectively. The field-induced resistance change has been attributed to the formation/rupture of the conducting filaments at the bottlenecks.

Acknowledgments

This work is supported by the National Key Projects for Basic Researches of China (2010CB923404), the National Natural Science Foundation of China (51172044), the National Science Foundation of Jiangsu Province of China (BK2011617), by NCET-09-0296, the Scientific Research Foundation for the Returned Overseas Chinese Scholars, State Education Ministry, and Southeast University (the Excellent Young Teachers Program and Seujq201106).

References

[1] M. Li, F. Zhuge, X. Zhu, K. Yin, J. Wang, Y. Liu, C. He, B. Chen, R. Li, Nanotechnology 21 (2010) 425202.
[2] K.M. Kim, G.H. Kim, S.J. Song, J.Y. Seok, M.H. Lee, J.H. Yoon, C.S. Hwang, Nanotechnology 21 (2010) 305203.
[3] H.Y. Peng, G.P. Li, J.Y. Ye, Z.P. Wei, Z. Zhang, D.D. Wang, G.Z. Xing, T. Wu, Appl. Phys. Lett. 96 (2010) 192113.
[4] X.T. Zhang, Q.X. Yu, Y.P. Yao, X.G. Li, Appl. Phys. Lett. 97 (2010) 222117.
[5] D. Lebeugle, A. Mougin, M. Viret, D. Colson, L. Ranno, Phys. Rev. Lett. 103 (2009) 257601.
[6] C.–H. Yang, J. Seidel, S.Y. Kim, P.B. Rossen, P. Yu, M. Gajek, Y.H. Chu, L.W. Martin, M.B. Holcomb, Q. He, P. Maksymovych, N. Balke, S.V. Kalinin, A.P. Baddorf, S.R. Basu, M.L. Scullin, R. Ramesh, Nat. Mater. 8 (2009) 485.
[7] S. Chen, J. Wu, Thin Solid Films 519 (2010) 499.
[8] K. Yin, M. Li, Y. Liu, C. He, F. Zhuge, B. Chen, W. Lu, X. Pan, R. Li, Appl. Phys. Lett. 97 (2010) 042101.
[9] X. Yuan, X. Xue, X. Zhang, Z. Wen, M. Yang, J. Du, D. Wu, Q. Xu, Solid State Commun. 152 (2012) 241.
[10] J. Allibe, I.C. Infante, S. Fusil, K. Bouzehouane, E. Jacquet, C. Deranlot, M. Bibes, A. Barthélémy, Appl. Phys. Lett. 95 (2009) 182503.
[11] L. Wei, Z. Li, W.F. Zhang, Appl. Surf. Sci. 255 (2009) 4992.
[12] C.D. Wagner, W.M. Riggs, L.E. Davis, J.F. Moulder, G.E. Mullenberg (Eds.), Perkin-Elmer Corporation, Minnesota, 1979.
[13] W. Chang, Y. Lai, T. Wu, S. Wang, F. Chen, M. Tsai, Appl. Phys. Lett. 92 (2008) 022110.
[14] Y.C. Yang, F. Pan, F. Zeng, M. Liu, J. Appl. Phys. 106 (2009) 123705.
[15] Q. Mao, Z. Ji, J. Xi, J. Phys. D: Appl. Phys. 43 (2010) 395104.
[16] H. Peng, T. Wu, Appl. Phys. Lett. 95 (2009) 152106.
[17] Y.C. Yang, F. Pan, Q. Liu, M. Liu, F. Zeng, Nano Lett. 9 (2009) 1636.
[18] Z. Yan, Y. Guo, G. Zhang, J.–M. Liu, Adv. Mater. 23 (2011) 1351.
[19] X. Qi, J. Dho, R. Tomov, Mark G. Blamire, Judith L. MacManus-Driscoll, Appl. Phys. Lett. 86 (2005) 062903.